TM-977
1100.000

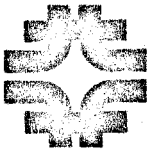

Fermilab

CALCULATIONS OF ENERGY DEPOSITION DENSITIES IN HIGH ENERGY ACCELERATOR TARGETS*

N.V. Mokhov** and A. Van Ginneken

June 19, 1980

I. Introduction

The calculation of energy deposition is of basic importance in understanding the behavior of matter irradiated by intense high-energy particle beams. The spatial distribution of the energy deposition density in a target is a starting point for further calculation concerning a variety of problems e.g. target heating, mechanical stability and development of shock waves.

This paper is a collection of recent results obtained for two specific design applications: (1) a target to maximize the anti-proton yield of proton beams in the 40 to 80 GeV energy range and (2) a beam dump capable of receiving up to 10^{14} protons per pulse of 1000 GeV maximum energy.

II. Calculations

Practically all detailed calculations of energy deposition proceed by tracing the hadronic shower via the Monte Carlo method. The dissipation of the shower's energy in the target can be divided into two parts (i) atomic ionization and excitation, virtually all of it caused by the charged particle members of the cascade and (ii) nuclear rearrangement whereby energy is expended in creating less

---

*Submitted to the Proceedings of the Workshop on High Intensity Targeting, Fermilab, April 1980
**Institute for High Energy Physics, Serpukhov, USSR

tightly bound nuclei and nuclear fragments from target nuclei. In almost all applications (including the present ones) only the former is assumed to contribute to the energy deposition.

The energy transfer from beam particles to atomic ionization and excitation of the medium can in turn be divided into four mechanisms: (i) electromagnetic showers, mainly from π^o decay into two photons, (ii) slowing down of the charged hadron constituents of the shower, (iii) nuclear de-excitation following collision and (iv) particles created or slowed down below the threshold of the calculation. Note that the division (ii)-(iv) is introduced for calculational reasons and is strongly dependent on the threshold energy (typically set in the 5-50 MeV region).

The calculations do not describe the behavior of the energy deposition by the shower as a function of time. The assumption that this takes place instantaneously is adequate for the present applications. (This ignores the relatively small contribution from long lived radioactivity.)

The main results presented here are obtained with the program CASIM[1] for hadronic showers coupled to program AEGIS[2] for tracing electromagnetic showers (this combination is hereafter referred to as MAXIM). For comparison results of a modified version of the MARS[3] code as well as with plain CASIM are included. The latter two simulate likewise the hadronic cascades but use phenomenological descriptions for the energy deposition of electromagnetic showers. Such descriptions are known to be suspect at small radial distances for high incident energies.[2] Figure 1 shows a comparison of CASIM and MARS with experimental results obtained from the observed temperature increase in segmented targets irradiated by 300 GeV protons.[4] Agreement of both codes with experiment is excellent. Figure 2

presents a comparison of MARS with MAXIM for the large energy densities encountered in a narrow region centered on the beam for the case of 80 GeV protons incident on BeO and Hg targets. (MAXIM results for Fe are also shown.) The beam distribution is Gaussian in both horizontal and vertical profile (uncorrelated) with standard derivation of σ_H = 0.06 mm and σ_v = 0.03 mm, respectively. The agreement is good for BeO throughout and at low depths also for Hg. At larger depths MARS predictions exceed those of MAXIM by up to 50%. From the jitter in the plot of Fig. 2 this discrepancy may well be largely statistical in origin. All three codes are compared in Fig. 3 for the case of 1000 GeV protons on a BeO target. Because of the high energy and small radii ($\leq$ 0.7 mm) involved the expected systematic derivations emerge. While CASIM and MARS agree quite well, MAXIM predicts energy densities larger by a factor of about 2.5.

All MAXIM results presented so far are obtained with the (standard) version of Refs. 1 and 2. For the present work two modifications are expressly introduced. The first concerns energy deposition by the low energy charged particles emitted via nuclear de-excitation or below threshold. Because the ranges of such particles exceed or are comparable to the small beam dimensions and radial bin sizes studied here it becomes necessary to introduce explicitely the spatial distribution of the energy deposited by these particles. (In the standard version their energy is deposited locally.)

The second modification is a calculational device. In the standard version one beam size and radial distribution as well as one fixed set of radial bins is chosen for each Monte Carlo run. In the present version a number of such beam distributions are analyzed simulatenously during the same Monte Carlo run. To accomplish this all incident particles are introduced along the beam axis. Then, whenever an

amount of energy is to be deposited at a certain location there is added to that location a vector chosen from the beam distribution. This process is then repeated for any desired number of beam distributions. To each distribution a different set of radial bins may be assigned. This procedure is strictly valid only for the case of complete translational symmetry in the radial direction. However it is a good approximation when the radial dimensions of both beam and bin size are small compared with the target radius and when the target is homogeneous in the radial direction, or at least well beyond the beam and bin dimensions. To simplify the computation further a single beam distribution vector is chosen for each incident particle and each component of this vector is then scaled for a set of (50) different beam distributions. The use of two or more such vectors and its influence on the convergence of the calculation is not explored. This scheme has obvious advantages in computer time economy versus repeated Monte Carlo runs. Another ingredient is that the energy densities deposited by different beams are fully correlated. This allows analysis of effects of beam size without most of the noise inherent in the Monte Carlo method. Some caution is required in interpretation since a smooth function of beam size may still have large overall statistical uncertainties.

III. Results

Figure 4 shows results for the central core of a Hg target, for two different beam sizes (vertical standard deviation, σ_V = 0.03 mm, horizontal standard deviation, σ_H = 0.06 mm for the first beam and $\sigma_V = \sigma_H$ = 0.07 mm for the second) and for 40 and 80 GeV incident protons. It is interesting to contrast results for the smaller beam at 80 GeV with the (MAXIM) results of Fig. 2. The difference reflects the modifications in the description of

energy deposition by low energy charged particles. For larger beams ($\sigma \gtrsim 1$ mm) the modification has negligible effects. The spatial distributions of energy density for graphite and Hg targets of a $\sigma_V = \sigma_H = 0.07$ mm beam of 80 GeV protons are shown in Figs. 5 and 6. At small radii the energy density derives almost completely from energy lost by the beam particles since secondaries are quickly lost from the central region. Figure 7 shows the radial dependence at two depths for a $\sigma_V = \sigma_H = 0.03$ mm beam of 80 GeV incident on Hg. At the small depth the shape of the energy density distribution follows closely that of the beam.

The maximum energy density in graphite and Hg targets as a function of beam area (defined as $4\pi\sigma_V\sigma_H$) is plotted in Fig. 8 for three different beam shapes ($\sigma_H = \sigma_V$, $\sigma_H = 2\sigma_V$ and $\sigma_H = 10\ \sigma_V$) and for 80 GeV incident protons. It is interesting that the results are completely independent of beam shape. Figure 9 shows the depth dependence of the energy density in the central core of the cascade for a series of beam sizes for the case of 1000 GeV protons on BeO. The shape of this depth dependence is seen to vary with increasing area from an exponential to that of a typical transition curve. The dependence of the maximum energy deposition in graphite as a function of beam area is shown in Fig. 10 for 80, 400 and 1000 GeV protons. At the low end of the area scale the maximum energy density for all three energies are seen to converge. This is a consequence of the fact that virtually all the energy is deposited by primary protons.

We wish to thank F. Turkot for discussion.

References

1. A. Van Ginneken, FNAL-FN-272, Batavia, IL (1975)

2. A. Van Ginneken, FNAL-FN-309, Batavia, IL (1978)

3. N.V. Mokhov, Proc. of IV All Union Conf. on Particle Accelerators, Moscow, Vol. 2, 222 (1975). I.S. Baishev, S.L. Kuchinin and N.V. Mokhov, Preprint IHEP-78-2, Serpukhov (1978)

4. M. Awschalom et al., Nucl. Inst. Meth., 131, 235 (1975)

Fig. 1 Energy density observed and calculated in Cu and W targets in the geometry of Ref. 4. The targets are a set of segmented cylinders 2.54 cm in diameter. The incident proton energy is 300 GeV.

Fig. 2 Energy density as a function of depth calculated in BeO, Cu and Hg targets for 80 GeV incident protons in central region (radius ≤ 0.015 mm) of target. The beam distribution is Gaussian in both horizontal and vertical profile with standard deviations of $\sigma_H = 0.06$ mm and (uncorrelated) $\sigma_V = 0.03$ mm, respectively. The abcissa expresses depth, z, as a fraction of the interaction length, λ ($\lambda_{BeO} = 29$ cm, $\lambda_{Fe} = 16$ cm, $\lambda_{Hg} = 13.5$ cm).

Fig. 3 Energy density in BeO target for 1000 GeV incident protons in central region (radius ≤ 0.7 mm) of target. The beam distribution is (uncorrelated) Gaussian in both horizontal and vertical profile with standard derivation of $\sigma_H = 1.4$ mm and $\sigma_V = 0.7$ mm, respectively.

Fig. 4 Energy density in Hg target for central region (radius ≤ 0.015 mm) for 40 and 80 GeV invident protons and beams of Gaussian profiles as indicated.

Fig. 5 Energy density in Hg target due to 80 GeV incident protons for the radial regions indicated. Beam has Gaussian profiles of $\sigma_H = \sigma_V = 0.07$ mm.

Fig. 6 Energy density in graphite target (density = 1.75 g cm^{-3}) due to 80 GeV incident protons for the radial regions indicated. Beam has Gaussian profiles of $\sigma_H = \sigma_V = 0.07$ mm.

Fig. 7 Energy density in Hg target as a function of radius for 80 GeV incident protons for a beam distribution of Gaussian profiles ($\sigma_H = \sigma_V = 0.03$ mm) and at the depths indicated.

Fig. 8 Maximum energy density for graphite (density = 1.75 g cm^{-3}) and Hg targets as a function of beam area for 80 GeV incident protons. The beams are of the shapes indicated and area is defined as $4\pi\sigma_H\sigma_V$. The maximum energy density is that observed in the central region (radius $\leq 0.5\ \sigma_V$).

Fig. 9 Energy density for BeO target in the central core (radius $\leq 0.5\ \sigma_V$) for 1000 GeV incident protons and for beam area ($\equiv 4\pi\sigma_H\sigma_V$) as indicated.

Fig. 10 Maximum energy density for graphite ($\rho = 1.75$ g cm^{-3}) targets as a function of beam area ($\equiv 4\pi\sigma_H\sigma_V$) for 80, 400 and 1000 GeV incident energy protons.

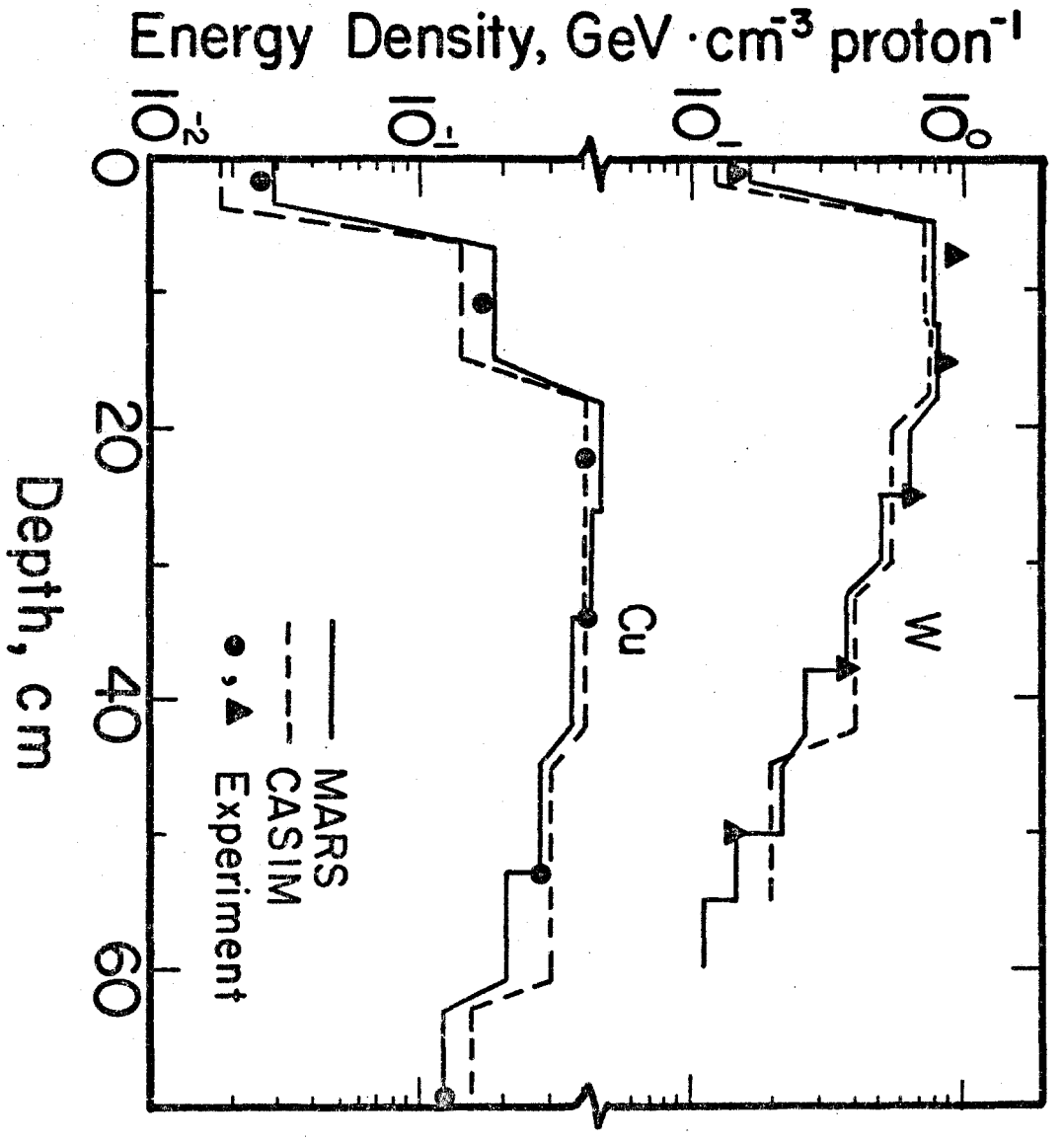
Energy Density, GeV·cm⁻³ proton⁻¹
10⁻²
10⁻¹
10⁻
10⁰
0
20
40
60
Depth, cm
MARS
CASIM
Experiment
Cu
W

Figure 1

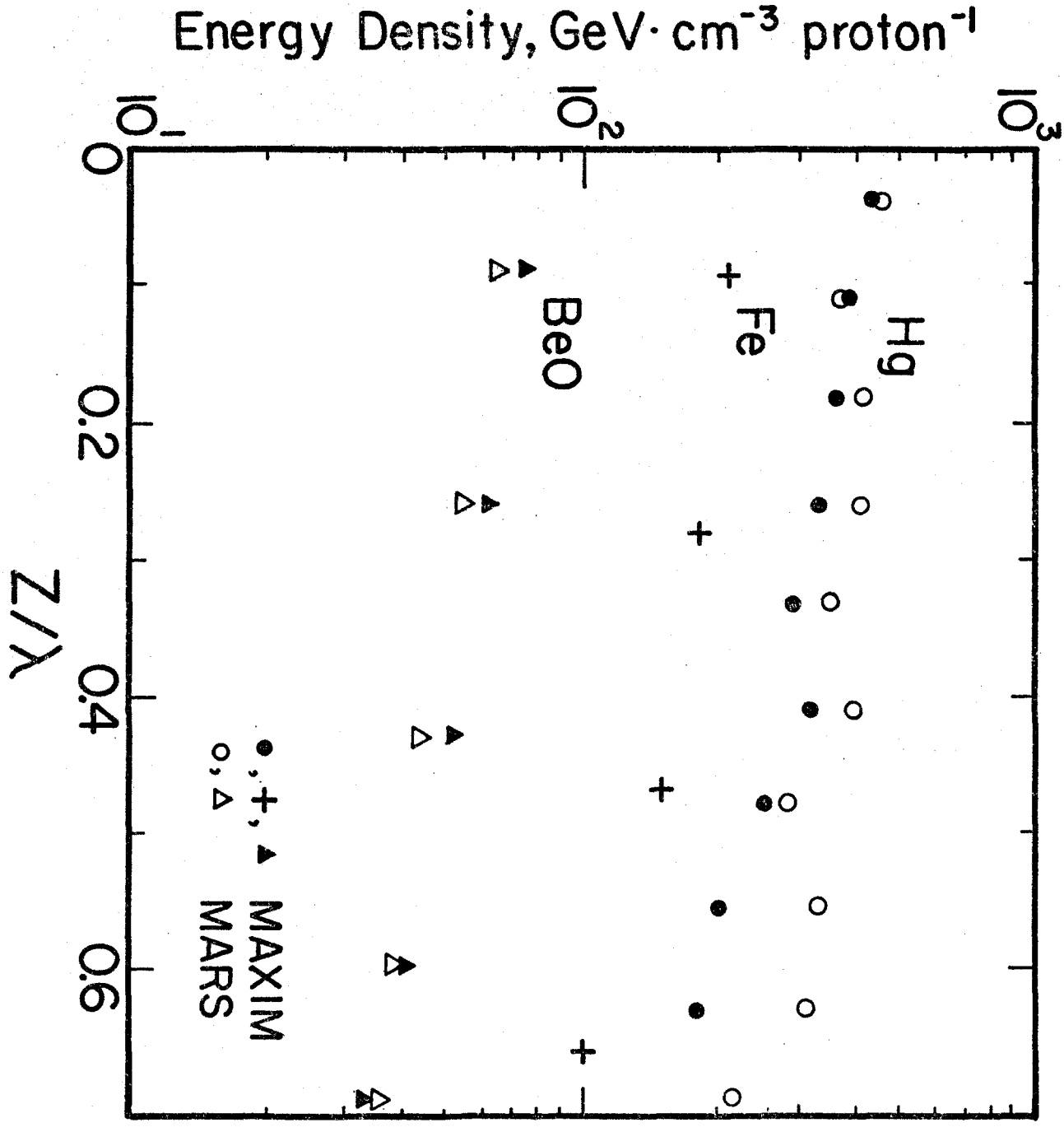
Energy Density, GeV·cm⁻³ proton⁻¹
10⁻
10₂
10³
0
0.2
0.4
0.6
Z/λ
BeO
Fe
Hg
●,+,▲ MAXIM
○,△ MARS

Figure 2

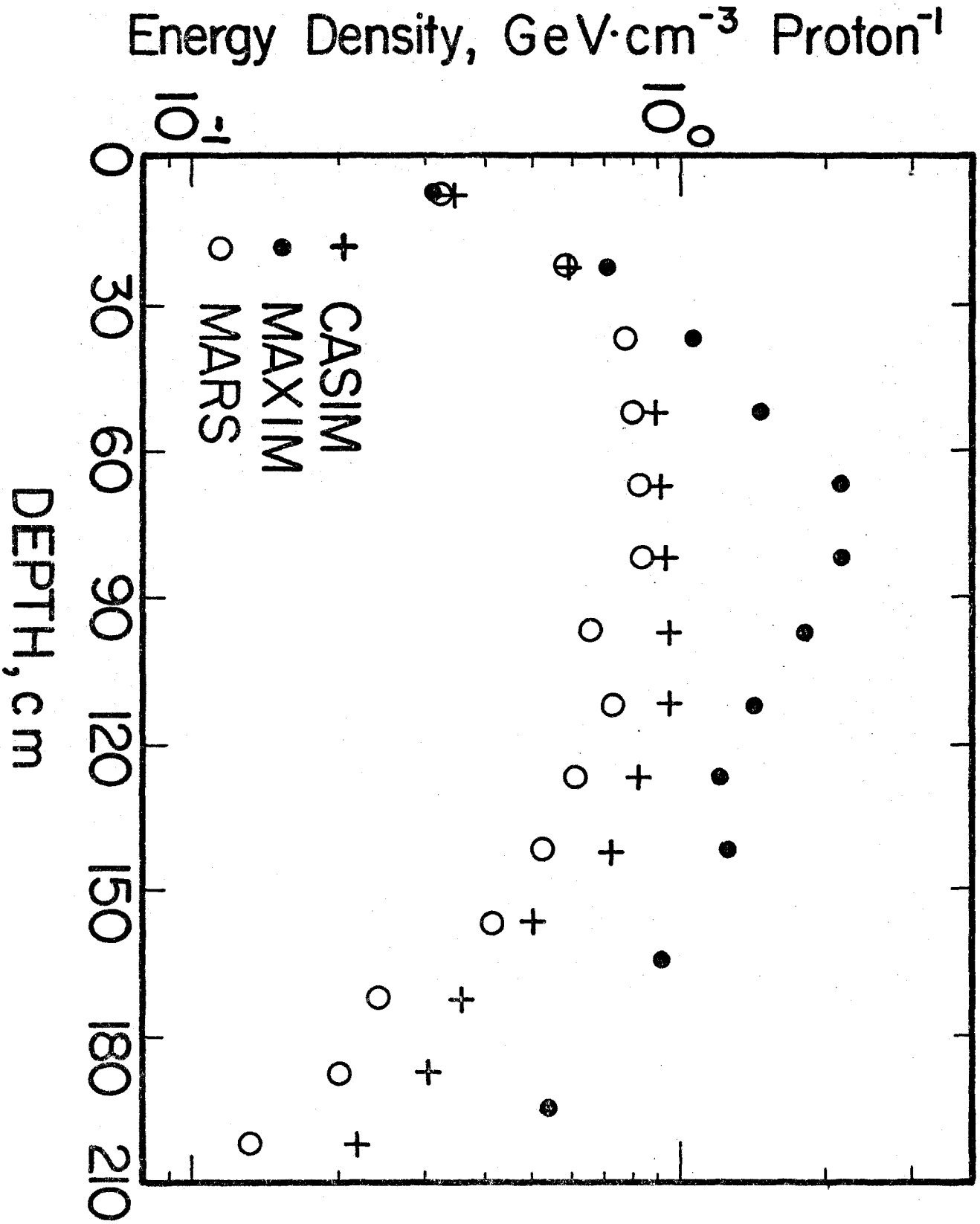
Energy Density, GeV·cm⁻³ Proton⁻¹
10⁻¹
10⁰
0
30
60
90
120
150
180
210
DEPTH, cm
CASIM
MAXIM
MARS

Figure 3

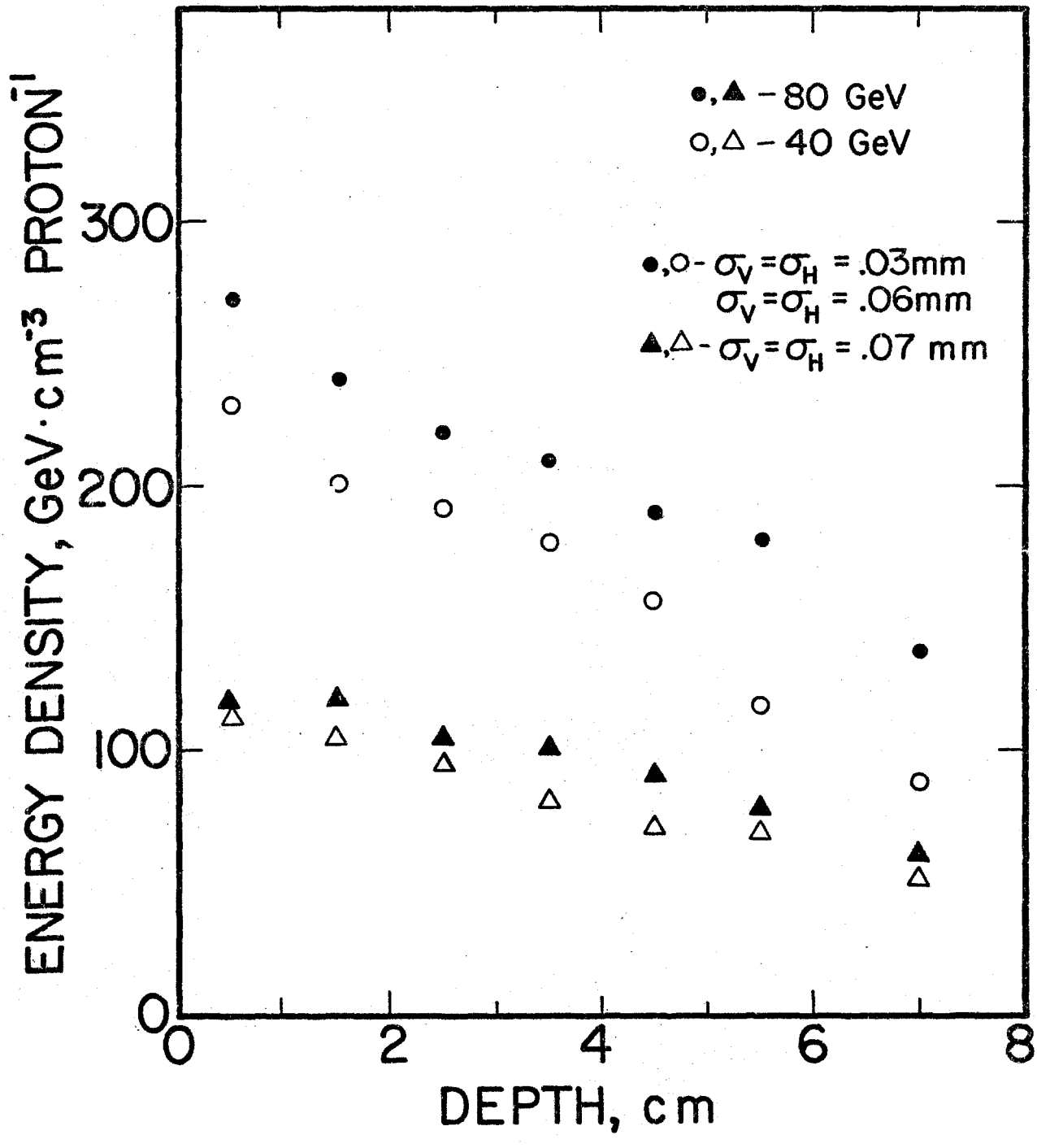
●,▲ - 80 GeV
○,△ - 40 GeV
●,○ - σV = σH = .03mm
σV = σH = .06mm
▲,△ - σV = σH = .07 mm
ENERGY DENSITY, GeV·cm⁻³ PROTON⁻¹
DEPTH, cm
0
100
200
300
0
2
4
6
8

Figure 4

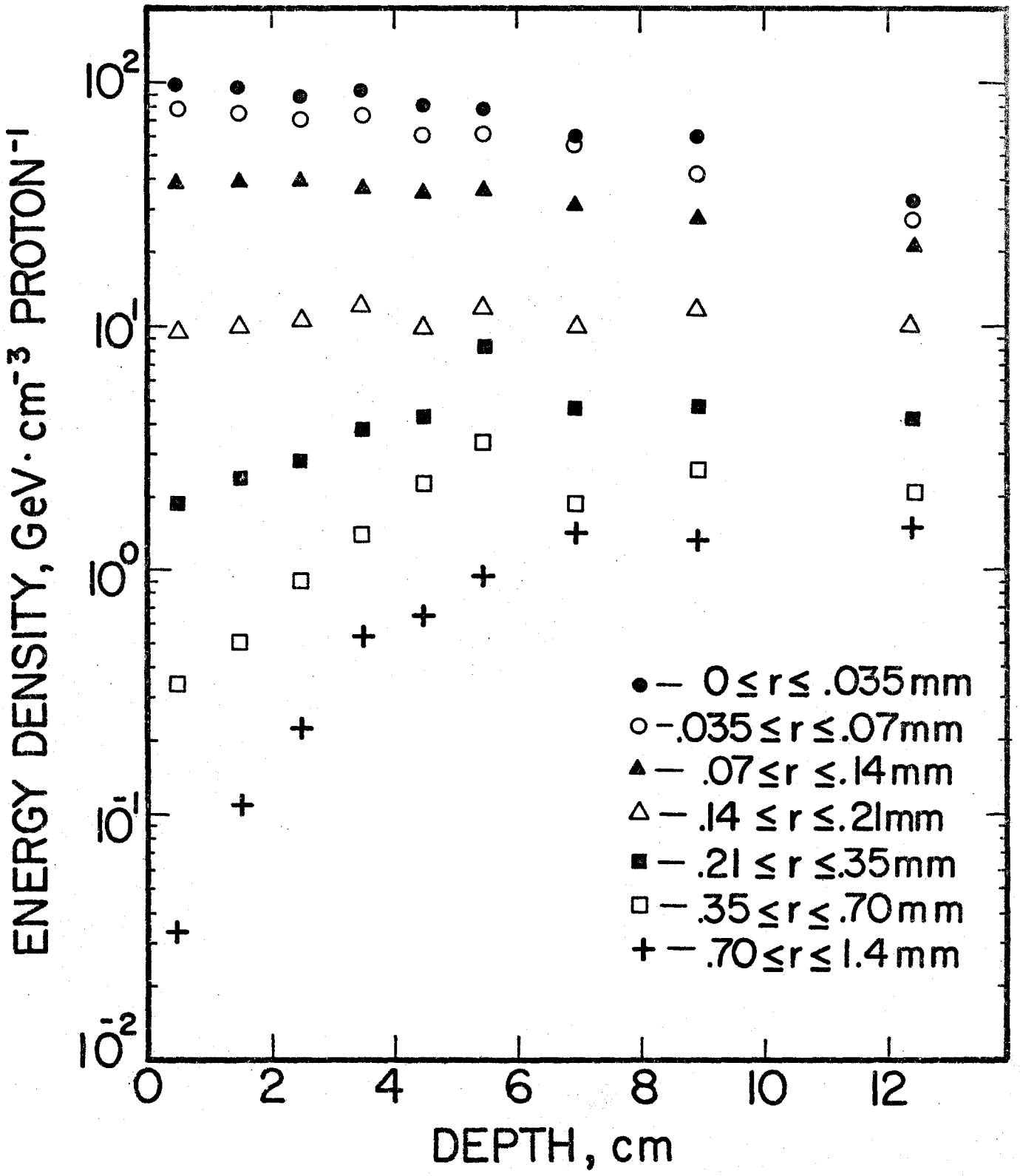
ENERGY DENSITY, GeV·cm⁻³ PROTON⁻¹
10²
10¹
10⁰
10⁻¹
10⁻²
0
2
4
6
8
10
12
DEPTH, cm
● — 0 ≤ r ≤ .035 mm
○ — .035 ≤ r ≤ .07 mm
▲ — .07 ≤ r ≤ .14 mm
△ — .14 ≤ r ≤ .21 mm
■ — .21 ≤ r ≤ .35 mm
□ — .35 ≤ r ≤ .70 mm
+ — .70 ≤ r ≤ 1.4 mm

Figure 5

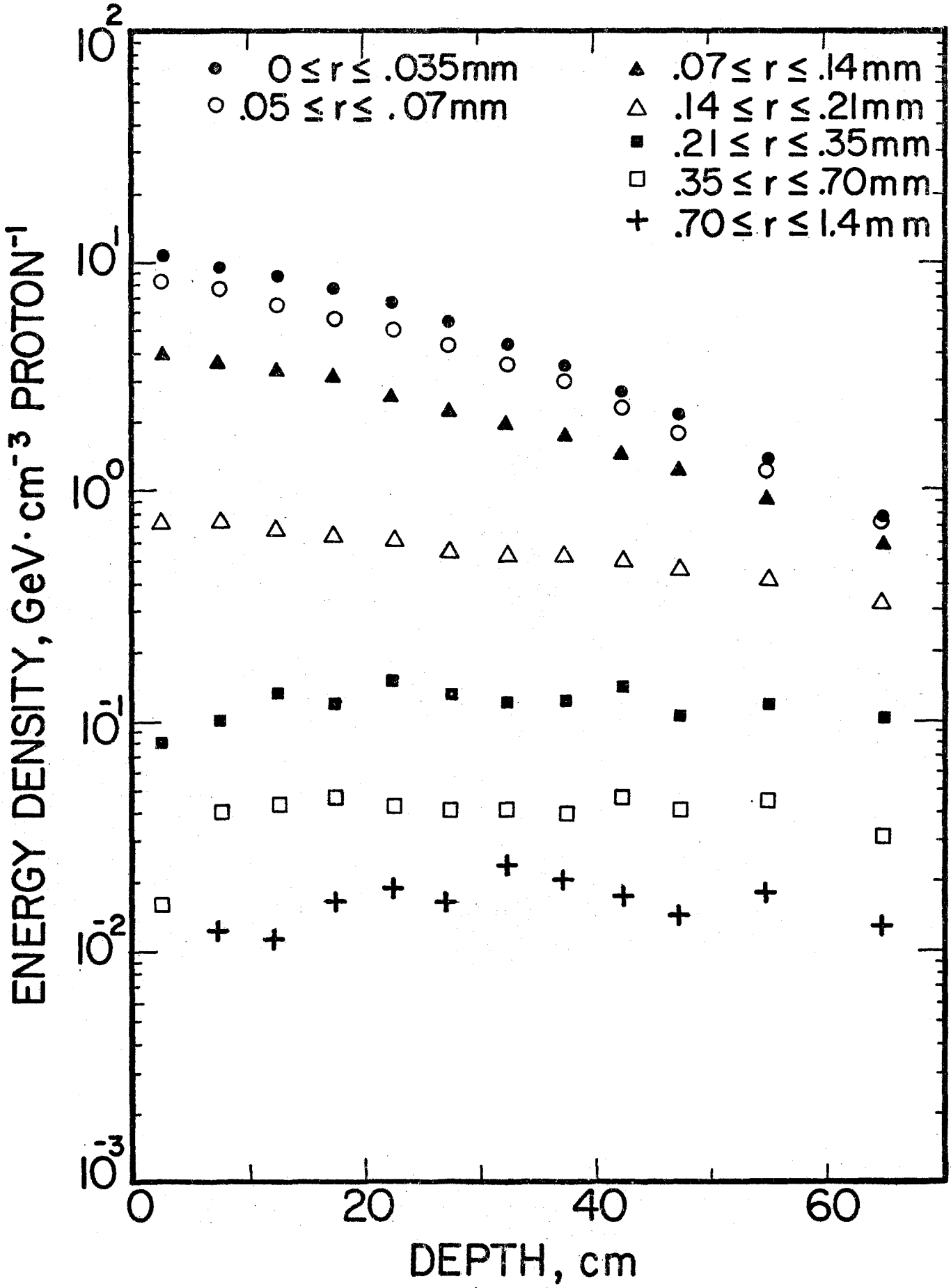
0 ≤ r ≤ .035mm
.05 ≤ r ≤ .07mm
.07 ≤ r ≤ .14mm
.14 ≤ r ≤ .21mm
.21 ≤ r ≤ .35mm
.35 ≤ r ≤ .70mm
.70 ≤ r ≤ 1.4mm
ENERGY DENSITY, GeV·cm⁻³ PROTON⁻¹
10²
10¹
10⁰
10⁻¹
10⁻²
10⁻³
0
20
40
60
DEPTH, cm

Figure 6

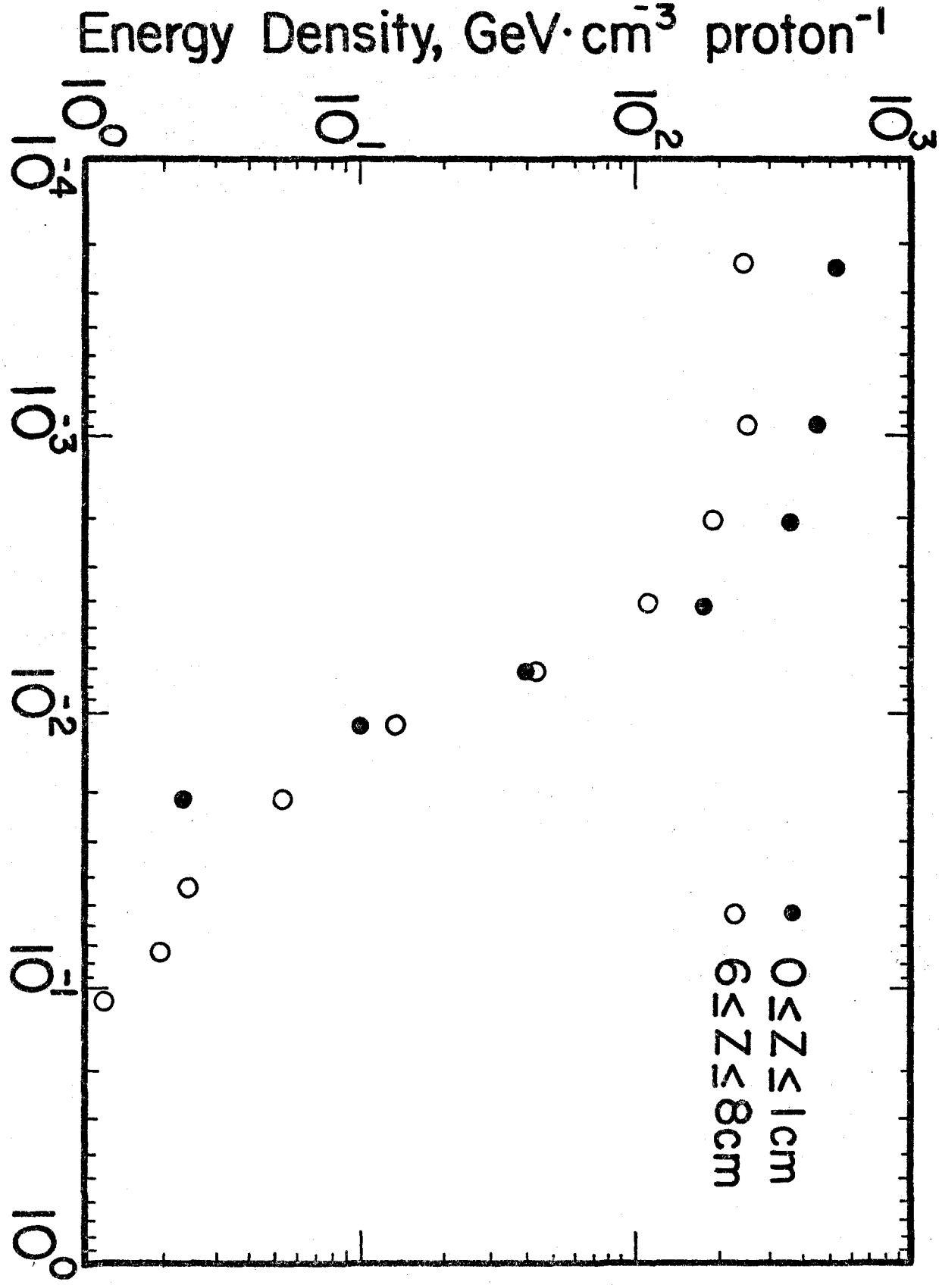
Energy Density, GeV·cm⁻³ proton⁻¹
10⁰
10⁻
10²
10³
10⁻⁴
10⁻³
10⁻²
10⁻¹
10⁰
RADIUS, cm
0≤Z≤1cm
6≤Z≤8cm

Figure 7

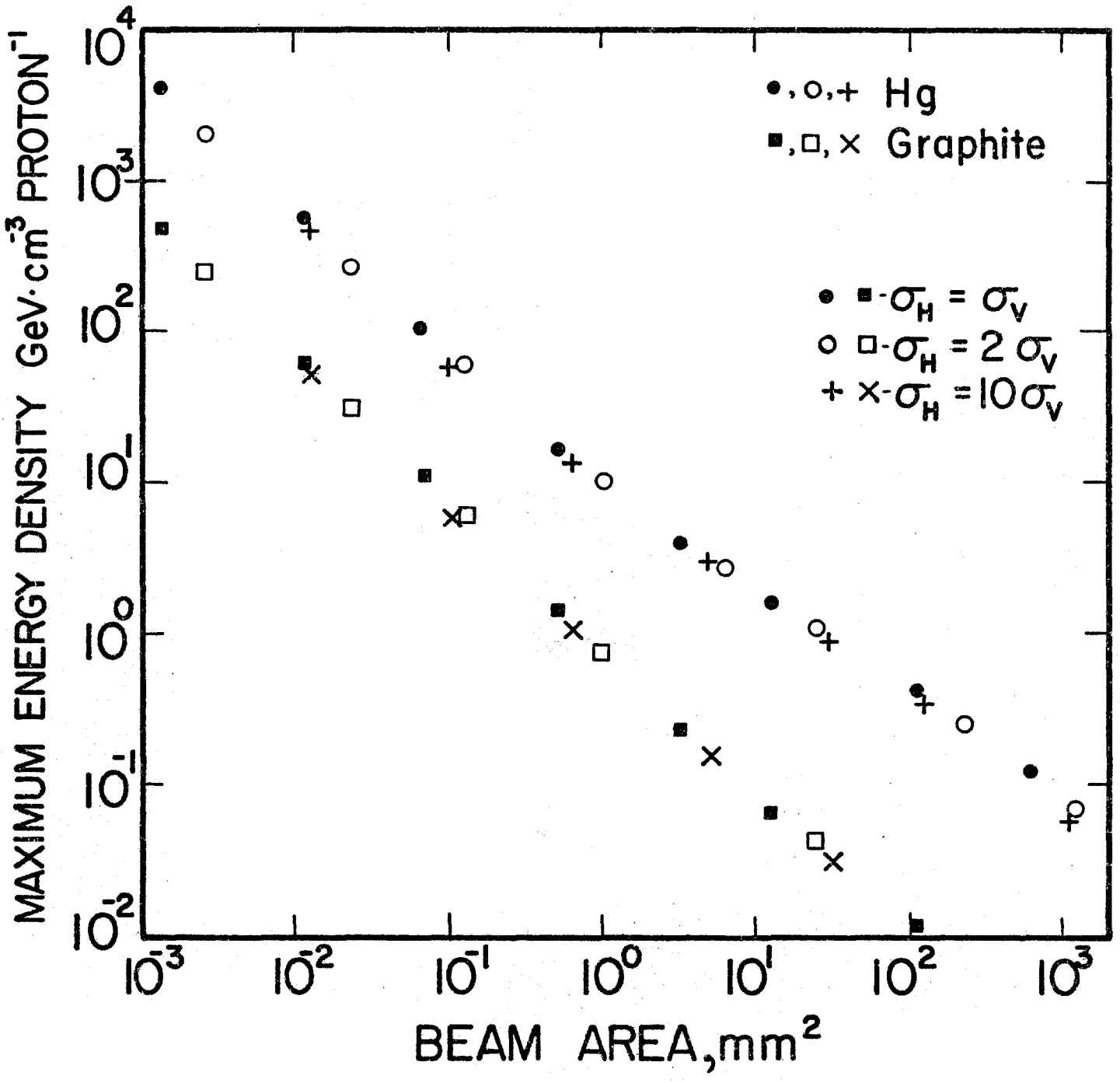
MAXIMUM ENERGY DENSITY GeV·cm⁻³ PROTON⁻¹
BEAM AREA, mm²
●, ○, + Hg
■, □, × Graphite
● ■ - σH = σV
○ □ - σH = 2 σV
+ × - σH = 10 σV

Figure 8

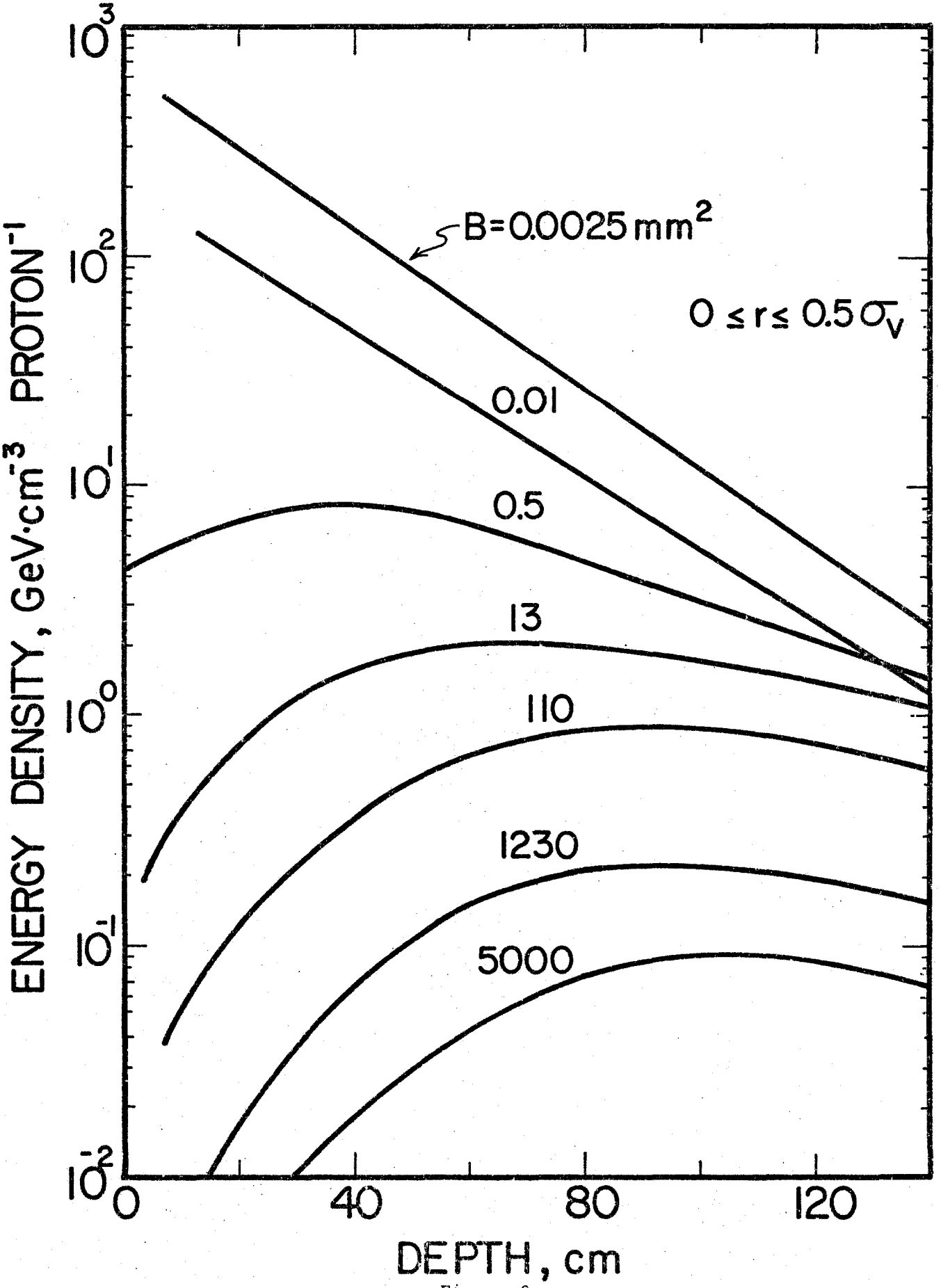
ENERGY DENSITY, GeV·cm⁻³ PROTON⁻¹
10³
10²
10
10⁰
10⁻¹
10⁻²
B=0.0025 mm²
0 ≤ r ≤ 0.5 σV
0.01
0.5
13
110
1230
5000
0
40
80
120
DEPTH, cm

Figure 9

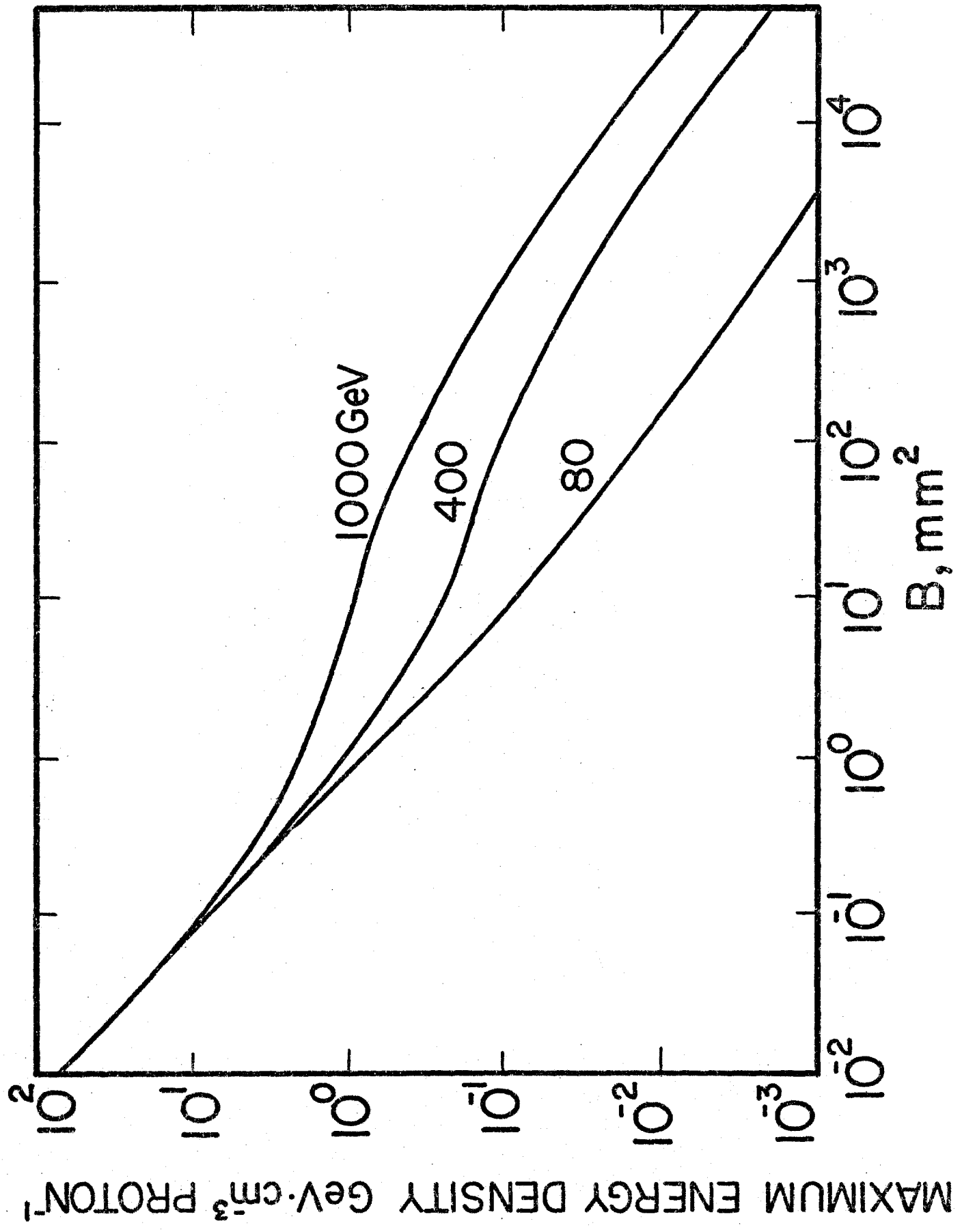
MAXIMUM ENERGY DENSITY GeV·cm⁻³ PROTON⁻¹
B, mm²
1000 GeV
400
80
10⁻²
10⁻¹
10⁰
10¹
10²
10³
10⁴

Figure 10